

Self-Assembly of Symmetric Diblock Copolymers  
in Planar Slits with and without Nanopatterns:  
Insight from Dissipative Particle Dynamics  
Simulations  
SUPPORTING INFORMATION

Pavel Petrus,<sup>1,2</sup> Martin Lísal,<sup>1,2,\*</sup> and John K. Brennan<sup>3</sup>

October 3, 2009

<sup>1</sup>*Department of Physics, Faculty of Science, J. E. Purkinje University, Ústí n. Lab., Czech Republic*

<sup>2</sup>*E. Hála Laboratory of Thermodynamics, Institute of Chemical Process Fundamentals of the ASCR, v. v. i., Prague 6-Suchbát, Czech Republic*

<sup>3</sup>*U.S. Army Research Laboratory, Weapons and Materials Research Directorate, Aberdeen Proving Ground, MD 21005-5066, U.S.A.*

\*Corresponding author.

E-mail: lisal@icpf.cas.cz

Mailing address: E. Hála Laboratory of Thermodynamics, Institute of Chemical Process Fundamentals of the ASCR, v. v. i., Rozvojová 135, 165 02 Prague 6-Suchbát, Czech Republic

Report Documentation Page				Form Approved OMB No. 0704-0188	
Public reporting burden for the collection of information is estimated to average 1 hour per response, including the time for reviewing instructions, searching existing data sources, gathering and maintaining the data needed, and completing and reviewing the collection of information. Send comments regarding this burden estimate or any other aspect of this collection of information, including suggestions for reducing this burden, to Washington Headquarters Services, Directorate for Information Operations and Reports, 1215 Jefferson Davis Highway, Suite 1204, Arlington VA 22202-4302. Respondents should be aware that notwithstanding any other provision of law, no person shall be subject to a penalty for failing to comply with a collection of information if it does not display a currently valid OMB control number.					
1. REPORT DATE <b>03 OCT 2009</b>		2. REPORT TYPE		3. DATES COVERED <b>00-00-2009 to 00-00-2009</b>	
4. TITLE AND SUBTITLE <b>Self-Assembly of Symmetric Diblock Copolymers in Planar Slits with and without Nanopatterns: Insight from Dissipative Particle Dynamics Simulations - Supporting Information</b>				5a. CONTRACT NUMBER	
				5b. GRANT NUMBER	
				5c. PROGRAM ELEMENT NUMBER	
6. AUTHOR(S)				5d. PROJECT NUMBER	
				5e. TASK NUMBER	
				5f. WORK UNIT NUMBER	
7. PERFORMING ORGANIZATION NAME(S) AND ADDRESS(ES) <b>E. Hala laboratory of Thermodynamics, Institute of Chemical Process Fundamentals of ASCR, v. v. i. Rozvojova 135, 165 02 Prague 6-Suchbát, Czech Republic,</b>				8. PERFORMING ORGANIZATION REPORT NUMBER	
9. SPONSORING/MONITORING AGENCY NAME(S) AND ADDRESS(ES)				10. SPONSOR/MONITOR'S ACRONYM(S)	
				11. SPONSOR/MONITOR'S REPORT NUMBER(S)	
12. DISTRIBUTION/AVAILABILITY STATEMENT <b>Approved for public release; distribution unlimited</b>					
13. SUPPLEMENTARY NOTES					
14. ABSTRACT					
15. SUBJECT TERMS					
16. SECURITY CLASSIFICATION OF:			17. LIMITATION OF ABSTRACT <b>Public Release</b>	18. NUMBER OF PAGES <b>18</b>	19a. NAME OF RESPONSIBLE PERSON
a. REPORT <b>unclassified</b>	b. ABSTRACT <b>unclassified</b>	c. THIS PAGE <b>unclassified</b>			

# 1 Planar Slits with Narrow, Vertically-Aligned Nanopatterns

We present the schematic phase diagram and some select nanostructures for narrow ( $L_{\text{NP}} = 6.25$ ), vertically-aligned nanopatterns in Figs. 1 and 2, respectively. Unlike the wide nanopatterned systems, the self-assembled nanostructures rather poorly follow the superposition description, with the exception at narrow slit widths and a few cases for slit widths between 6 and 10. For these narrow nanopatterned planar slits, the nanopatterns have a greater influence on the overall self-assembly of the diblock copolymers, where we observed the formation of novel nanostructures such as  $L_{\parallel,1}+L_{\perp}$  (Fig. 2a) and  $L_{\parallel,1}+L_{\parallel,1}^{-1}$  (Fig. 2c). Overall for  $W > 10$ , the system forms either lamellar phases corresponding to the  $w_1$ -portion of the nanopatterned planar slits, e.g.,  $L_{\parallel,\nu}$ 's or a chevron-like lamellar phase (Fig. 2b) (mainly for  $\Delta a_{Bw_2}/\Delta a_{AB} = 0$ ), or tilt-like lamellar phases (Fig. 2d) for both  $\Delta a_{Bw_2}/\Delta a_{AB} = 0.5$  and 1. Additional DPD simulations with boxlengths  $L_x = 25$  and  $L_y = 20$  resulted in a different structure only for  $[W, \Delta a_{Bw_2}/\Delta a_{AB}] = [16, 0]$ , where a chevron-like lamellar phase formed instead of  $L_{\perp}$  (both nanostructures are indicated in Fig. 1, separated by comma). Here again, it occurs at a microphase separation boundary between two different types of nanostructures, which explains the ambiguity due to highly pronounced finite-size and commensurate effects.

# 2 Planar Slits with Narrow, Vertically-Staggered Nanopatterns

The schematic phase diagram and some select nanostructures for narrow ( $L_{\text{NP}} = 6.25$ ), vertically-staggered nanopatterns are displayed in Figs. 3 and 4, respectively. Unlike the wide, vertically-staggered nanopatterns but similar to the narrow, vertically-aligned nanopatterns, the resulting nanostructures do not obey the superposition behavior of lamellar alignment in planar slits without nanopatterns (i.e., in planar slits with  $w_1$ - and  $w_2$ -walls), except for a few cases. For these narrow, vertically-staggered nanopatterns, the systems spontaneously form novel  $L+iL$  (Fig. 4a) and  $L-L_{\parallel,1}+iL-L_{\parallel,1}$  (Fig. 4b) nanostructures. Overall for wide slit widths, in addition to the formation of  $L_{\perp}$  phases, the systems exhibit nanostructures characterized by a mixture of parallel and tilt lamellae (Fig. 4c) or exclusively tilt-like lamellar phases (Fig. 4d). Additional DPD simulations with boxlengths  $L_x = 25$  and  $L_y = 20$  resulted in different nanostructures for the cases of  $[W, \Delta a_{Bw_2}/\Delta a_{AB}] = \{[11, 0], [17, 0], [16, 0.5]\}$ , with formations of a  $L_{\perp}$  phase instead of a  $L-L_{\parallel,1}+iL-L_{\parallel,1}$  phase, a  $L_{\parallel,3}$  phase instead of a parallel-tilt lamellar phase, and a tilt-like lamellar phase instead of a parallel-tilt lamellar phase, respectively. The nanostructures

that formed for the different-sized simulation cells are indicated in Fig. 3, separated by comma. All of these cases occur at microphase separation boundaries between two different types of nanostructures, which explains the ambiguity due to highly pronounced finite-size and commensurate effects.

### 3 Planar Slits with Vertically-Partially-Staggered Nanopatterns

#### 3.1 Wide Nanopatterns ( $L_{\text{NP}} = 12.5$ )

The schematic phase diagram and some select nanostructures for wide, vertically-partially-staggered nanopatterns are shown in Figs. 5 and 6. Unlike the previous wide nanopatterned systems, the self-assembled nanostructures rather poorly follow the superposition description, with the exception at very narrow slit widths and a few cases for wider nanopatterned planar slits. In contrast to vertically-aligned or vertically-staggered nanopatterns, where the superposition description is given by the phase behavior in planar slits with  $w_1$ -walls or in planar slits with  $w_1$ - and  $w_2$ -walls, respectively, here the superposition description combines the phase behavior in both planar slits with  $w_1$ -walls and planar slits with  $w_1$ - and  $w_2$ -walls. The actual size of the  $w_1$ -partitions and  $w_1$ - and  $w_2$ -partitions of the nanopatterned planar slits is  $L_{\text{NP}}/2$ , i.e., not sufficient for the systems at wide slit widths ( $W > 5$ ) to develop nanostructures corresponding to particular partitions of the nanopatterned planar slits. This fact is supported by the observed nanostructures at  $W = 7$  and  $8$  when  $\Delta a_{Bw_2}/\Delta a_{AB} = 0$  and  $0.5$ , and at  $W = 13$  and  $14$  when  $\Delta a_{Bw_2}/\Delta a_{AB} = 0$ , which obey the superposition description even at wider slit widths. However, this is due to the appearance of parallel alignment in three successive partitions of the nanopatterned planar slits. Therefore at wider slit widths, we mostly see parallel lamellar phases (for  $\Delta a_{Bw_2}/\Delta a_{AB} = 0$ ) or chevron-like (Fig. 6d) and/or tilt-like (Fig. 6e) lamellar phases. For narrow slit widths up to  $5$ , the system nearly follows the superposition description and forms perpendicular lamellar phases for  $W = 2$  and  $3$ , and a nanostructure given by a combination of adsorbed layer, inverted adsorbed layer and perpendicular phases (denoted as  $L+L_{\perp}+iL+L_{\perp}$ , and shown in Fig. 6a). The wide, vertically-partially-staggered nanopatterns generated two unique nanostructures at  $W = 10$  and  $11$  when  $\Delta a_{Bw_2}/\Delta a_{AB} = 0$ . The nanostructure at  $W = 10$  is formed by a tilt of  $L_{\perp}$  to smoothly join the  $iL-L_{\parallel,1}$  and  $L-L_{\parallel,1}$  phases (denoted as  $iL-L_{\parallel,1}+tL_{\parallel,1}+L-L_{\parallel,1}+L_{\perp}$  and shown in Fig. 6b), while the nanostructure at  $W = 11$  results from a tilt of  $L_{\parallel,2}$  and  $L_{\perp}$  to smoothly join  $iL-L_{\parallel,1}$  and  $L-L_{\parallel,1}$  phases (denoted as  $iL-L_{\parallel,1}+tL_{\parallel,1}+L-L_{\parallel,1}+tL_{\parallel,1}$  and shown in Fig. 6c). Additional DPD simulations with boxlengths  $L_x = 25$

and  $L_y = 20$  resulted in a different structure only for  $[W, \Delta a_{Bw_2}/\Delta a_{AB}] = [17, 0]$ , which lies at a microphase separation boundary between two different types of nanostructures. The nanostructures that formed for the different-sized simulation cells are indicated in Fig. 5, separated by comma.

### 3.2 Narrow Nanopatterns ( $L_{NP} = 6.25$ )

The schematic phase diagram and some select nanostructures for narrow, vertically-partially-staggered nanopatterns are shown in Figs. 7 and 8. Analogous to the wide, vertically-partially-staggered nanopatterned case, the systems obey the superposition description only at very narrow slit widths ( $W < 6$ ), where the systems exhibit  $L_\perp$  phases for  $W = 2$  and 3(4), and  $L+L_\perp+iL+L_\perp$  phases (Fig. 8a) otherwise. For wide slit widths, the systems mostly form tilt-like lamellar phases (Fig. 8c). Additionally though, the systems self-assemble into  $L_{\parallel,\nu}$  phases when  $\Delta a_{Bw_2}/\Delta a_{AB} = 0$  and into  $L_\perp$  phases for a few cases. The narrow, vertically-partially-staggered nanopatterns also generated unique nanostructures at  $[W, \Delta a_{Bw_2}/\Delta a_{AB}] = \{[9, 0], [7, 0.5]\}$  formed by a succession of  $L_{\parallel,1}$  and  $L_\perp$  phases (denoted as  $L_{\parallel,1}+L_\perp+L_{\parallel,1}+L_\perp$  and shown in Fig. 8b).

## 4 Conformational Behavior in the Nanopatterned Planar Slits

Figs. 9 and 10 show examples of diblock copolymer conformational behavior in terms of the nematic order parameter,  $P_{2,d}$ , for the planar slits with vertically-aligned and vertically-staggered nanopatterns, respectively. Abrupt changes in the orientational order are clearly exhibited during the transformation between phases.

Figure 1: Self-assembly of the  $A_5B_5$  systems confined in nanopatterned planar slits, where strips on opposing surfaces are vertically aligned with size  $L_{NP} = 6.25$ .  $W$  is the slit width and  $\Delta a_{Bw_2}/\Delta a_{AB}$  is a measure of phobicity of the B-blocks towards the  $w_2$ -walls. Schematics indicate lamellar alignment in the planar slits without nanopatterns, i.e., in planar slits with  $w_1$ -walls.  $w_1$ - and  $w_2$ -walls are represented by black and blue lines, respectively. Crosses indicate cases where nanostructures did not result from superposition of the lamellar alignment in the underlying planar slits without nanopatterns. Letters (a)-(d) refer to simulation configurations for some select nanostructures formed in the nanopatterned planar slits, which are shown in Fig. 2. Other legend definitions are:  $L_{\perp}$ , a perpendicular lamellar phase; and  $L_{\parallel,\nu}$ , parallel lamellar phases with  $\nu$  A-lamellae. For the case in which different nanostructures were observed for different-sized simulation cells, both nanostructures are shown separated by comma.

Figure 2: Examples of simulation configurations corresponding to Fig. 1. (a)  $L_{\parallel,1}+L_{\perp}$ ; (b) chevron-like lamellar phase; (c)  $L_{\parallel,1}+L_{\parallel,1}^{-1}$ ; and (d) tilt-like lamellar phase. Shown in the inset of (c) are isosurfaces for the A-beads. Green and gold spheres represent A- and B-beads, respectively, while grey and pink spheres represent  $w_1$ - and  $w_2$ -wall beads, respectively. B-beads are not shown in (a) and (c) for visual clarity.

Figure 3: Self-assembly of the  $A_5B_5$  systems confined in nanopatterned planar slits, where strips on opposing surfaces are vertically staggered with size  $L_{NP} = 6.25$ .  $W$  is the slit width and  $\Delta a_{Bw_2}/\Delta a_{AB}$  is a measure of phobicity of the B-blocks towards the  $w_2$ -walls. Schematics indicate lamellar alignment in planar slits without nanopatterns, i.e., in the planar slits with  $w_1$ - and  $w_2$ -walls.  $w_1$ - and  $w_2$ -walls are represented by black and blue lines, respectively. Crosses indicate cases where nanostructures did not result from superposition of the lamellar alignment in the underlying planar slits without nanopatterns. Letters (a)-(d) refer to simulation configurations for some select nanostructures formed in the nanopatterned planar slits, which are shown in Fig. 4. Other legend definitions are:  $L_{\perp}$ , a perpendicular lamellar phase; and  $L_{\parallel,3}$ , a parallel lamellar phase with three A-lamellae. For cases in which different nanostructures were observed for different-sized simulation cells, both nanostructures are shown separated by comma.

Figure 4: Examples of simulation configurations corresponding to Fig. 3. (a)  $L+iL$ ; (b)  $L_{\parallel,1}+iL-L_{\parallel,1}$ ; (c) parallel-tilt lamellar phase; and (d) tilt-like lamellar phase. Shown in the insets of (a) and (b) are isosurfaces for the A-beads. Green spheres represent A-beads, while grey and pink spheres represent  $w_1$ - and  $w_2$ -wall beads, respectively. B-beads are not shown for visual clarity.

Figure 5: Self-assembly of the  $A_5B_5$  systems confined in nanopatterned planar slits, where strips on opposing surfaces are vertically partially staggered with size  $L_{NP} = 12.5$ .  $W$  is the slit width and  $\Delta a_{Bw_2}/\Delta a_{AB}$  is a measure of phobicity of the B-blocks towards the  $w_2$ -walls. Schematics indicate lamellar alignment in the planar slits without nanopatterns, i.e., in the planar slits with  $w_1$ -walls and in the planar slits with  $w_1$ - and  $w_2$ -walls.  $w_1$ - and  $w_2$ -walls are represented by black and blue lines, respectively. Crosses indicate cases where nanostructures did not result from superposition of the lamellar alignment in the underlying planar slits without nanopatterns. Letters (a)-(e) refer to simulation configurations for some select nanostructures formed in the nanopatterned planar slits, which are shown in Fig. 6. Other legend definitions are:  $L_{\perp}$ , a perpendicular lamellar phase;  $L_{\parallel,\nu}$ , a parallel lamellar phase with  $\nu$  A-lamellae; \*, a phase given by a succession of  $L_{\perp}/L_{\parallel,1}/L_{\perp}/L_{\perp}$  phases in the particular partitions of these nanopatterned slits; and \*\*, a phase given by a succession of  $L_{\perp}/L_{\parallel,1}/L_{\parallel,1}/L_{\perp}$  phases in the particular partitions of these nanopatterned slits. For the case in which different nanostructures were observed for different-sized simulation cells, both nanostructures are shown separated by comma.

Figure 6: Examples of simulation configurations corresponding to Fig. 5. (a)  $L+L_{\perp}+iL+L_{\perp}$ ; (b)  $iL-L_{\parallel,1}+tL_{\parallel,1}+L-L_{\parallel,1}+L_{\perp}$ ; (c)  $iL-L_{\parallel,1}+tL_{\parallel,1}+L-L_{\parallel,1}+tL_{\parallel,1}$ ; (d) chevron-like lamellar phase; and (e) tilt-like lamellar phase. Also shown are insets of isosurfaces for the A-beads. Green and gold spheres represent A- and B-beads, respectively, while grey and pink spheres represent  $w_1$ - and  $w_2$ -wall beads, respectively.

Figure 7: Self-assembly of the  $A_5B_5$  systems confined in nanopatterned planar slits, where strips on opposing surfaces are vertically partially-staggered with size  $L_{NP} = 6.25$ .  $W$  is the slit width and  $\Delta a_{Bw_2}/\Delta a_{AB}$  is a measure of phobicity of the B-blocks towards the  $w_2$ -walls. Schematics indicate lamellar alignment in the planar slits without nanopatterns, i.e., in the planar slits with  $w_1$ -walls and in the planar slits with  $w_1$ - and  $w_2$ -walls.  $w_1$ - and  $w_2$ -walls are represented by black and blue lines, respectively. Crosses indicate cases where nanostructures did not result from superposition of the lamellar alignment in the underlying planar slits without nanopatterns. Letters (a)-(c) refer to simulation configurations for some select nanostructures formed in the nanopatterned planar slits, which are shown in Fig. 8. Other legend definitions are:  $L_{\perp}$ , a perpendicular lamellar phase; and  $L_{\parallel,\nu}$ , a parallel lamellar phase with  $\nu$  A-lamellae.

Figure 8: Examples of simulation configurations corresponding to Fig. 7. (a)  $L+L_{\perp}+iL+L_{\perp}$ ; (b)  $L_{\parallel,1}+L_{\perp}+L_{\parallel,1}+L_{\perp}$ ; and (c) tilt-like lamellar phase. Also shown are insets of isosurfaces for the A-beads. Green and gold spheres represent A- and B-beads, respectively, while grey and pink spheres represent  $w_1$ - and  $w_2$ -wall beads, respectively.

Figure 9: The nematic order parameter,  $P_{2,d}$ , as a function of the slit width,  $W$ , for the  $A_5B_5$  copolymers confined in nanopatterned planar slits, where strips on opposing surfaces are vertically aligned with size (a)  $L_{NP} = 12.5$  and (b)  $L_{NP} = 6.25$ ; and where  $\Delta a_{Aw_1}/\Delta a_{AB} = \Delta a_{Bw_2}/\Delta a_{AB} = 1$ . Symbols represent simulation results, where dotted lines are drawn as a guide to the eye and vertical dashed lines mark approximate microphase separation boundaries. Other legend definitions are:  $L_{\perp}$ , a perpendicular lamellar phase; the letters (a), (e) and (g) in Fig. 9a refer to the nanostructures shown in Fig. 10 of the paper; letters (c) and (d) in Fig. 9b refer to the nanostructures shown in Fig. 1.



Figure 10: The nematic order parameter,  $P_{2,d}$ , as a function of the slit width,  $W$ , for the  $A_5B_5$  copolymers confined in nanopatterned planar slits, where strips on opposing surfaces are vertically staggered with size (a)  $L_{NP} = 12.5$  and (b)  $L_{NP} = 6.25$ ; and where  $\Delta a_{Aw_1}/\Delta a_{AB} = \Delta a_{Bw_2}/\Delta a_{AB} = 1$ . Symbols represent simulation results, where dotted lines are drawn as a guide to the eye and vertical dashed lines mark approximate microphase separation boundaries. Other legend definitions are:  $L_{\perp}$ , a perpendicular lamellar phase; letters (a)-(c) in Fig. 10a refer to the nanostructures shown in Fig. 12 of the paper; letters (a) and (d) in Fig. 10b refer to the nanostructures shown in Fig. 3.

Fig. 1 (Petrus et al.)

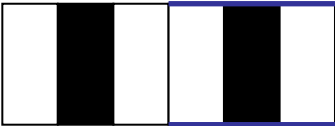
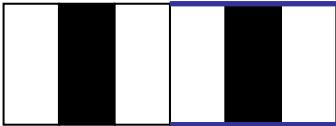
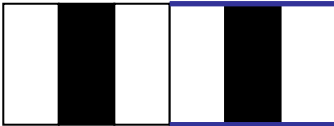


























$W$	$\Delta a_{Bw2} / \Delta a_{AB} = 0$	$\Delta a_{Bw2} / \Delta a_{AB} = 0.5$	$\Delta a_{Bw2} / \Delta a_{AB} = 1$	
2				
3				
4				
5				
6	 <span>a</span>	 <span><math>L_{\perp}</math></span>	 <span><math>L_{\perp}</math></span>	
7	 <span><math>L_{\parallel,1}</math></span>	 <span>a</span>	 <span>c</span>	
8		 <span>c</span>		
9	 <span>a</span>	 <span>c</span>		
10			 <span>c</span>	
11	 <span><math>L_{\perp}</math></span>	 <span><math>L_{\perp}</math></span>	 <span><math>L_{\perp}</math></span>	
12	 <span><math>L_{\parallel,2}</math></span>			
13	 <span><math>L_{\parallel,2}</math></span>	 <span>d</span>		 <span>d</span>
14				
15	 <span><math>L_{\perp}, b</math></span>	 <span><math>L_{\perp}</math></span>		
16	 <span>b</span>			
17	 <span><math>L_{\parallel,3}</math></span>	 <span><math>L_{\parallel,3}</math></span>	 <span>d</span>	
18		 <span>d</span>		
19				
20				

Fig. 2 (Petrus et al.)

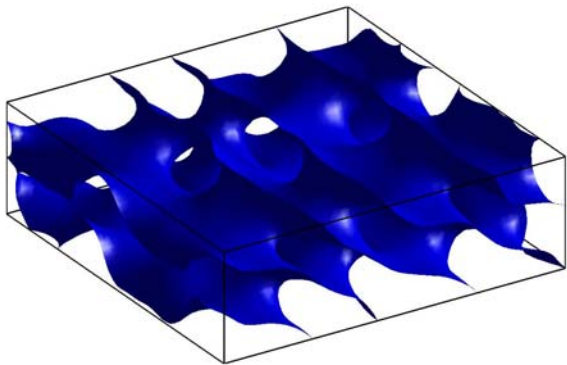
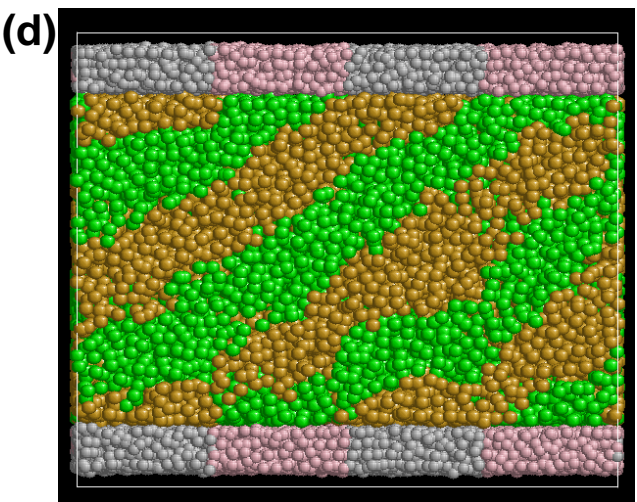
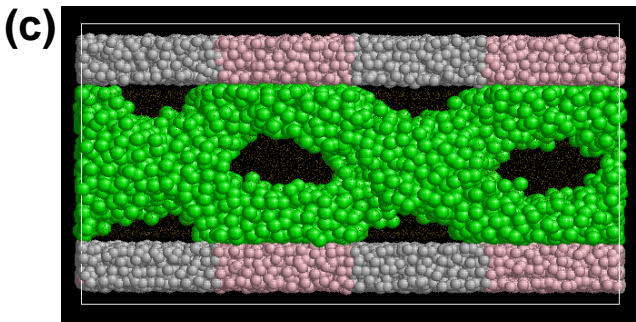
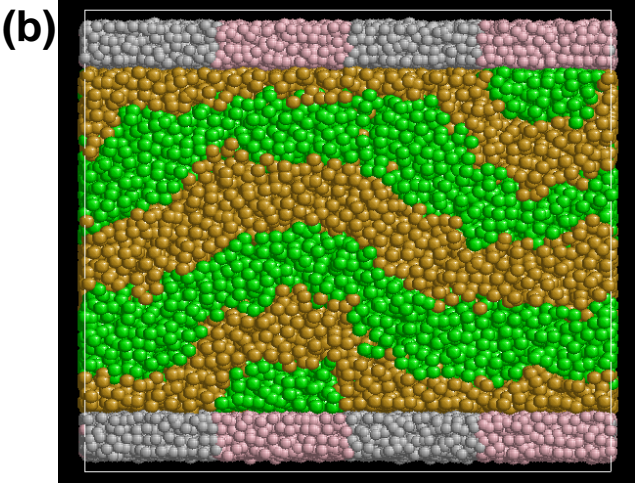
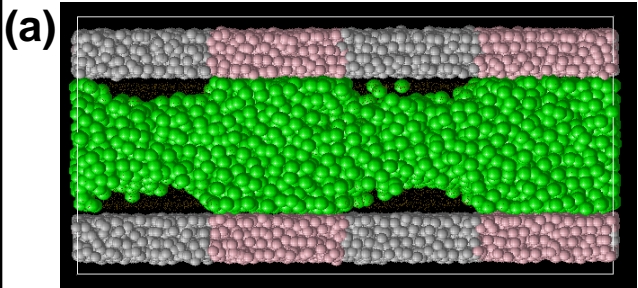


Fig. 3 (Petrus et al.)

$W$	$\Delta a_{Bw2} / \Delta a_{AB} = 0$	$\Delta a_{Bw2} / \Delta a_{AB} = 0.5$	$\Delta a_{Bw2} / \Delta a_{AB} = 1$
2			
3			
4			
5			
6			
7			
8			
9			
10			
11			
12			
13			
14			
15			
16			
17			
18			
19			
20			



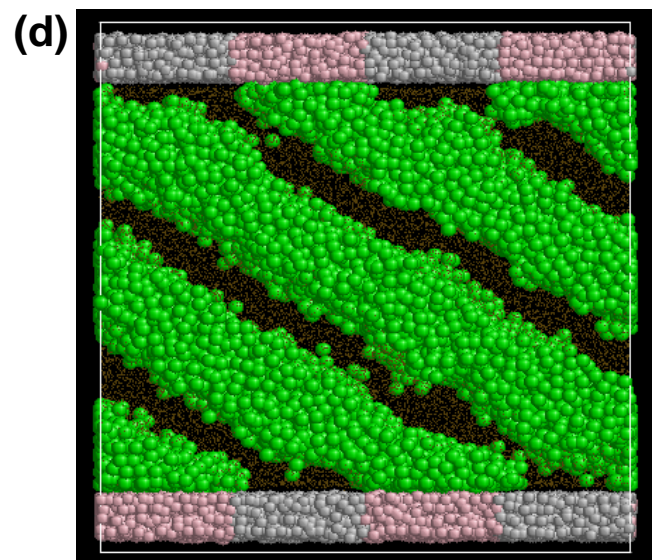
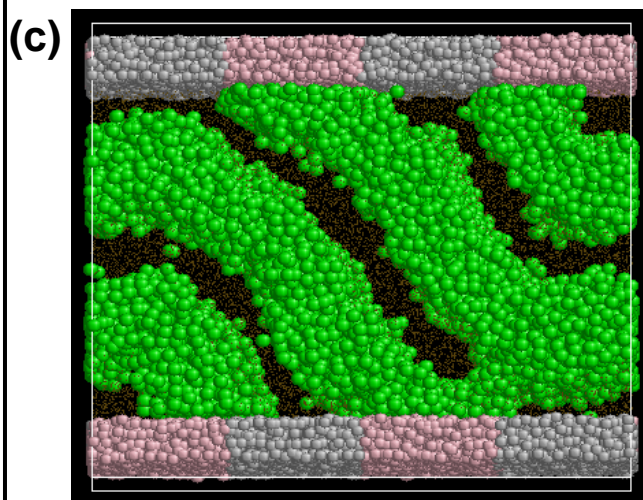
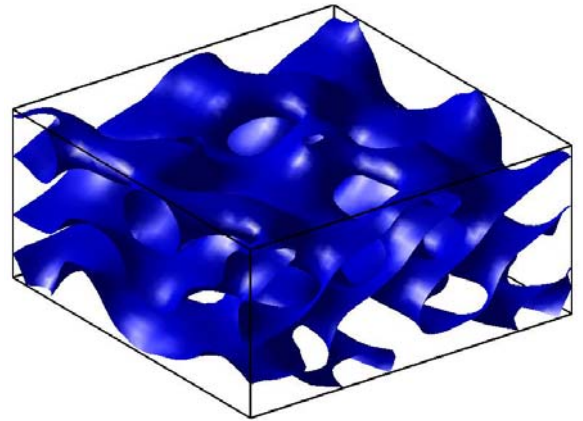
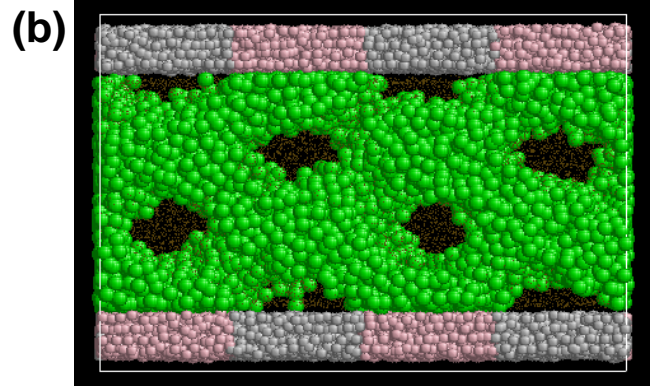
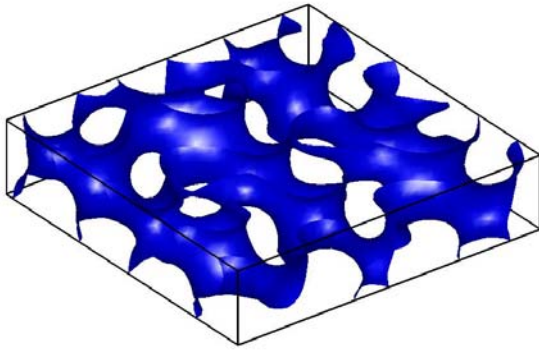
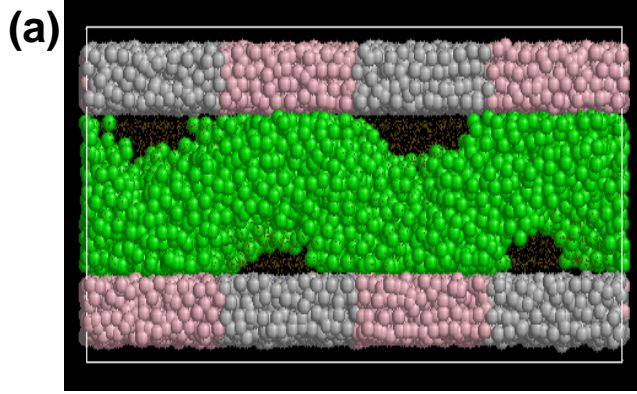
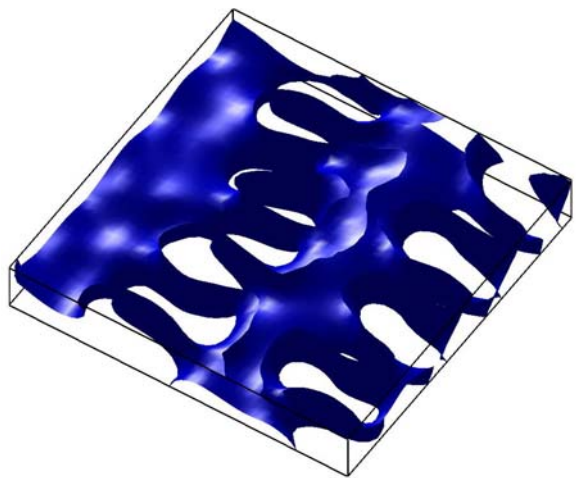
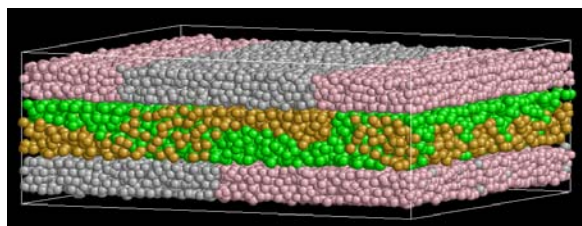


Fig. 5 (Petrus et al.)

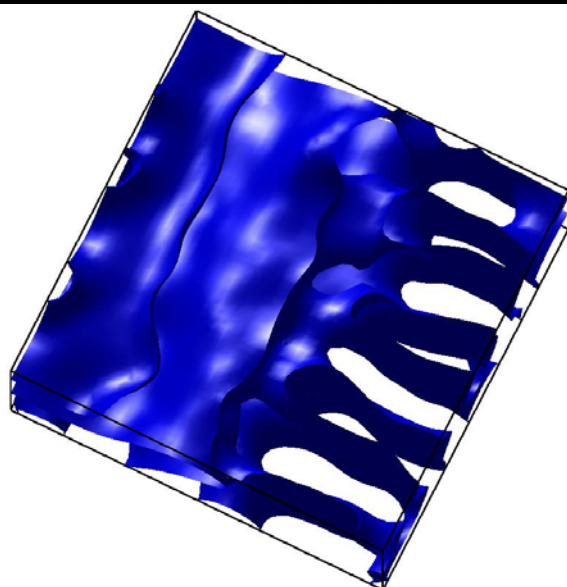
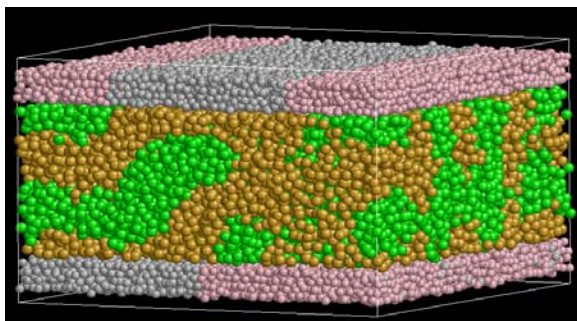
$W$	$\Delta a_{Bw2} / \Delta a_{AB} = 0$	$\Delta a_{Bw2} / \Delta a_{AB} = 0.5$	$\Delta a_{Bw2} / \Delta a_{AB} = 1$
2			
3		 	
4	 	 	 
5	 	 	 
6	 	 	 
7			
8			
9	 	 	 
10	 	 	 
11	 	 	 
12	 	 	 
13		 	
14			
15	 	 	 
16	 	 	 
17	 	 	 
18	 	 	 
19	 	 	 
20	 	 	 



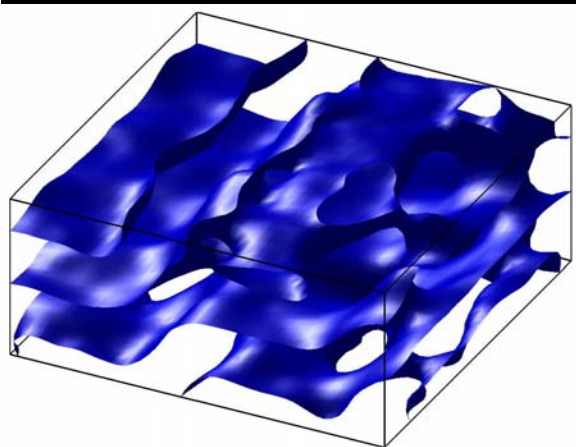
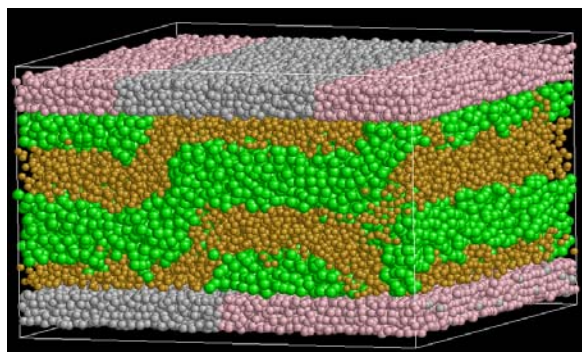
(a)



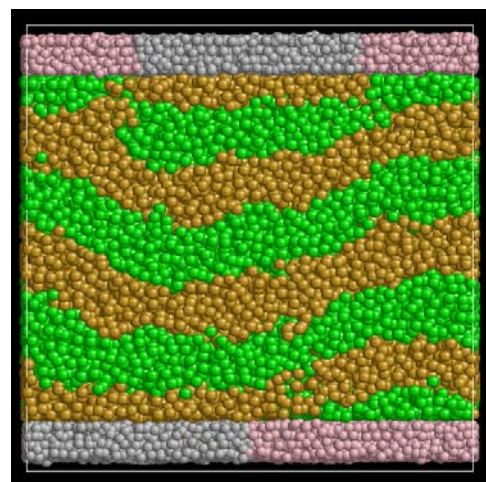
(b)



(c)



(d)



(e)

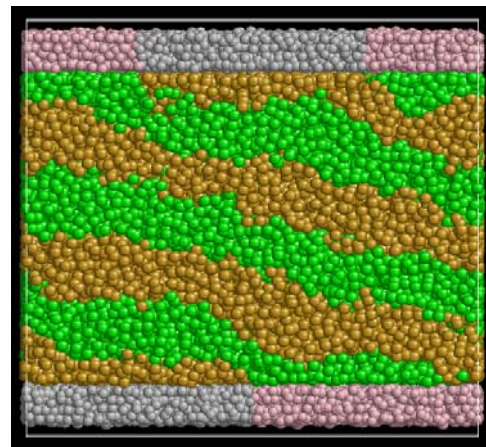
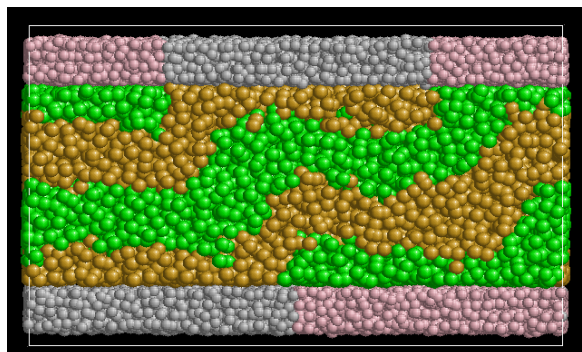


Fig. 7 (Petrus et al.)

$W$	$\Delta a_{Bw2} / \Delta a_{AB} = 0$	$\Delta a_{Bw2} / \Delta a_{AB} = 0.5$	$\Delta a_{Bw2} / \Delta a_{AB} = 1$
2			
3			
4			
5			
6			
7			
8			
9			
10			
11			
12			
13			
14			
15			
16			
17			
18			
19			
20			



Fig. 8 (Petrus et al.)

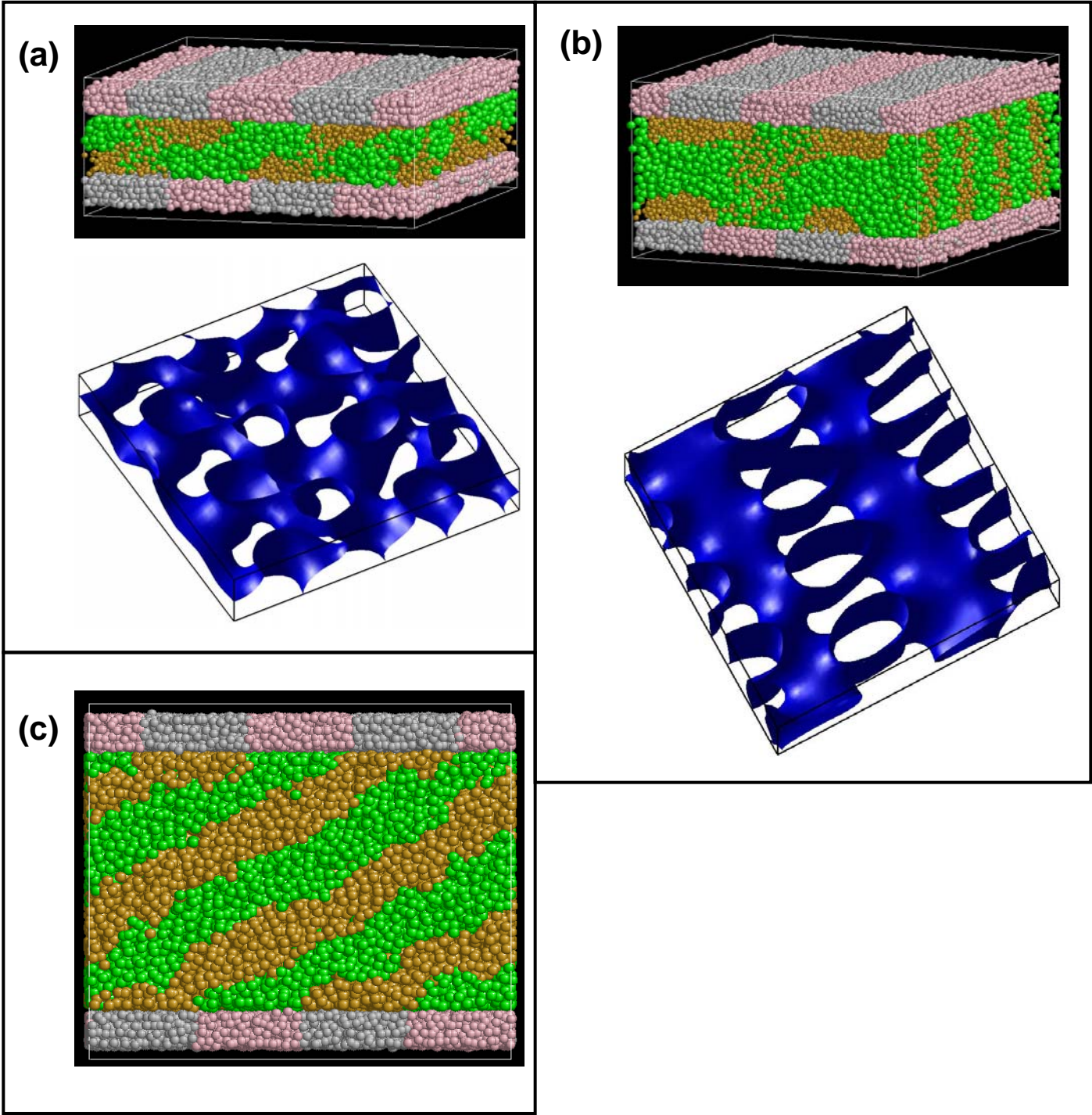


Fig. 9 (Petrus et al.)

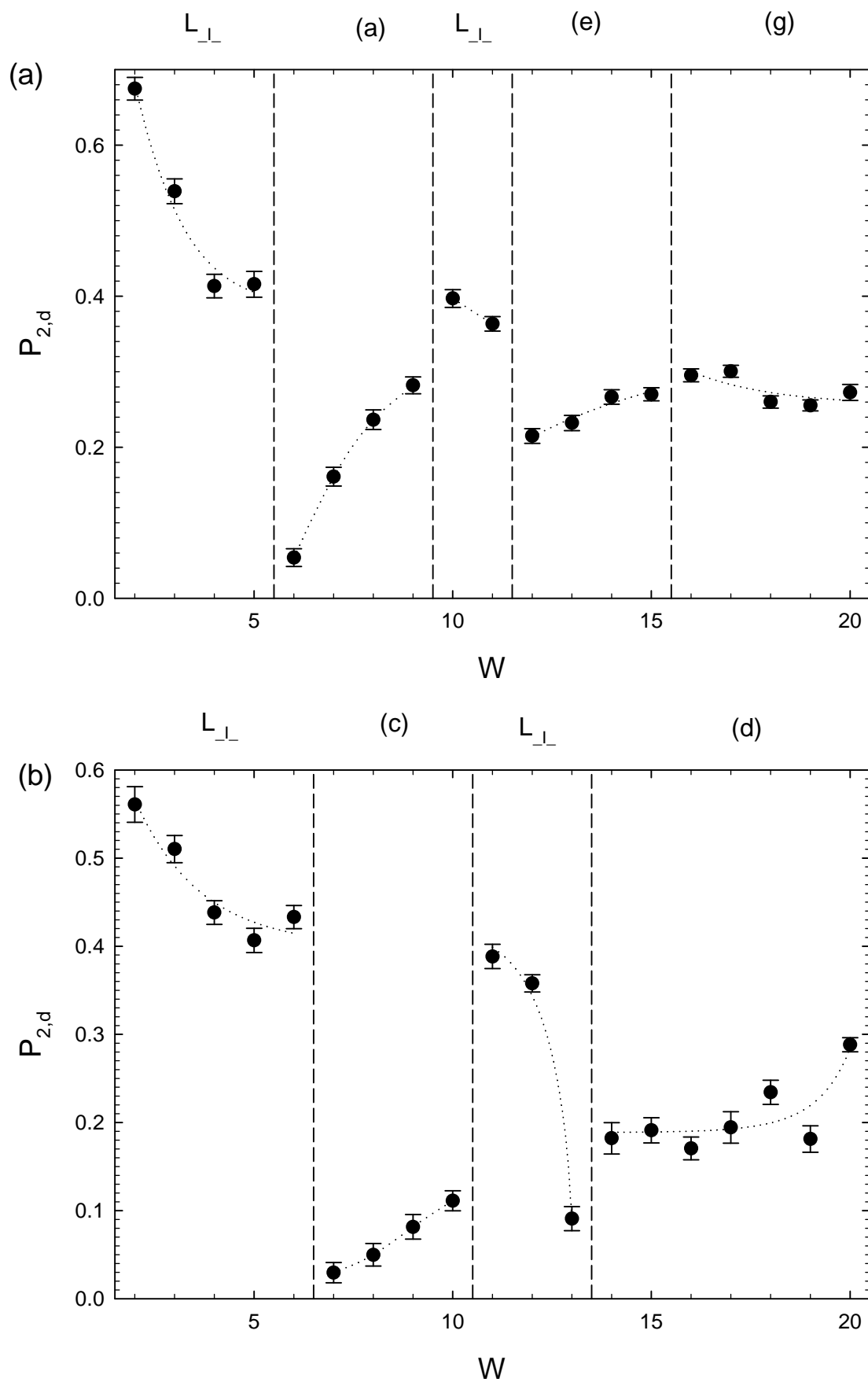


Fig. 10 (Petrus et al.)

